Metastable structure of $Li_{13}Si_4$

Thomas Gruber, Silvia Bahmann, and Jens Kortus
TU Bergakademie Freiberg, Institut für Theoretische Physik, Leipziger Strasse 23, 09596 Freiberg, Germany
(Received 20 November 2015; revised manuscript received 27 January 2016; published 6 April 2016)

The $Li_{13}Si_4$ phase is one out of several crystalline lithium silicide phases, which is a potential electrode material for lithium ion batteries and contains a high theoretical specific capacity. By means of *ab initio* methods like density functional theory (DFT) many properties such as heat capacity or heat of formation can be calculated. These properties are based on the calculation of phonon frequencies, which contain information about the thermodynamical stability. The current unit cell of "$Li_{13}Si_4$" given in the ICSD database is unstable with respect to DFT calculations. We propose a modified unit cell that is stable in the calculations. The evolutionary algorithm EVO found a structure very similar to the ICSD one with both of them containing metastable lithium positions. Molecular dynamic simulations show a phase transition between both structures where these metastable lithium atoms move. This phase transition is achieved by a very fast one-dimensional lithium diffusion and stabilizes this phase.

DOI: 10.1103/PhysRevB.93.144104

I. INTRODUCTION

There is a huge need in our society for new battery materials, which results in increasing research effort in that area [1–3]. Lithium silicides are promising electrode materials due to high theoretical specific capacity of over 3500 mAh g^{-1} [4,5]. The biggest challenge for application is the capacity loss during lithiation and delithiation due to a large volume change of about 400% [6,7]. Not surprisingly this results in a poor cyclability over the full capacity range [8,9]. Crack formation in the electrode material after several cycles [10] is, for example, one major problem. Lithium silicides have been investigated as electrode materials and NMR measurements during the Li exchange process reveal crystalline structures such as $Li_{13}Si_4$ [11,12].

The thermodynamic properties of the known crystalline Li-Si phases have been evaluated based on experimental data by Wang *et al.* [13]. Modern state-of-the-art *ab initio* methods based on density functional theory (DFT) can also calculate many properties like heat capacity, thermal expansion coefficients, or formation energy. Additionally, these methods are also capable of searching for new possible crystal structures, which may come up during lithiation [14] but have not been identified yet.

New structures can be induced by lithium diffusion and insertion. Some progress has been made to understand the lithiation process starting from pure silicon [7,15,16]. However, to understand the whole lithiation process the diffusion pathways are important, which may be different compared to pure silicon [17].

The lithiation process has been simulated before by inserting lithium atoms step by step in silicon bulk material [18], nanowires [19], and on different crystalline sites [20] with geometry optimization between the insertions. Another approach is molecular dynamic (MD) by filling the simulation cell either with a silicon cluster surrounded by lithium atoms [21] or with a bulk silicon structure on one side and lithium atoms on the other side [22]. The crystalline starting material often changes in amorphous structures, therefore the MD calculations often start with amorphous silicon structures [23].

Information on lithium diffusion is highly interesting for use as battery material and can be obtained from MD. The lithium diffusion in the case of amorphous structures is of the order of $D = 10^{-9}$ cm^2 s^{-1} [22]. In contrast, the diffusion can be much faster in crystalline lithium silicides as was observed experimentally for $Li_{12}Si_7$ [24].

We have used an evolutionary algorithm called EVO [25], which was developed in our group to search for new structures in the Li-Si system and to improve the understanding of the phase diagram. This search yielded indeed a new possible crystal structure in the case of the $Li_{13}Si_4$ phase. Further, we present MD studies to investigate lithium diffusion for $Li_{13}Si_4$. The new structure found by EVO and also seen in our MD runs during the 1D lithium diffusion study in the $Li_{13}Si_4$ phase differs from the structure given in the ICSD database. Section II explains the investigated crystal structures in detail, Sec. III delivers information on computational details, and the results will be discussed in Sec. IV.

II. CRYSTAL STRUCTURES OF $Li_{13}Si_4$

A. Structure from the ICSD database

The starting structure we used for our investigation was published by Frank *et al.* [26] and can be found in the ICSD database (ICSD-660135) with space group 55 (Pbam). The structure has an orthorhombic crystal system and contains only two different layers of atoms in the *ab* plane, one with silicon dimers and one with single silicon atoms, which are surrounded by 12 lithium atoms. They form a polyhedron, which looks like a distorted icosahedron [Fig. 1(a)] with six lithium atoms in the same plane as the silicon atom. The other six atoms form the top and bottom triangle, which are not rotated with respect to each other around the *c* axis.

The silicon dimer is surrounded by a Li_6 ring in chair conformation perpendicular to the Si-Si bond [Fig. 2(a)]. Parallel to the ring there are four lithium atoms in rhombohedral arrangement at each end of the dimer.

See Supplemental Material for the crystal structure file [27].

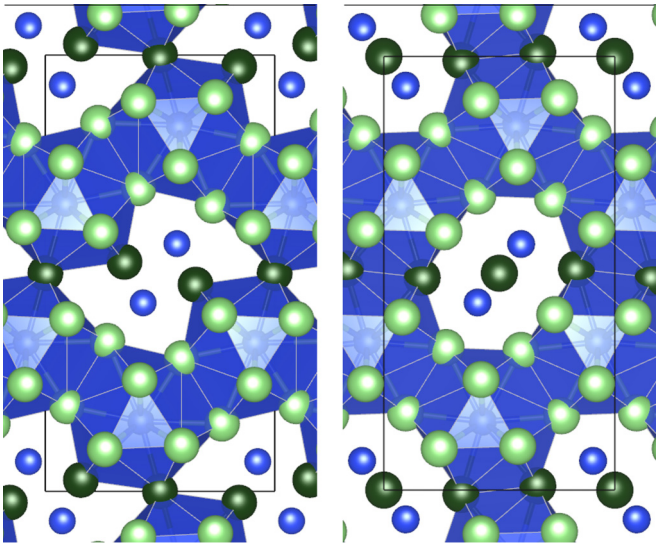

(a) from ICSD database (b) obtained with EVO

FIG. 1. Crystal structures of $Li_{13}Si_4$ with c axis pointing toward the viewer (Li, light + dark green; Si, blue). Light reflections produces bright surfaces. The structures can be converted into each other by shifting the dark-green lithium atoms in the direction of the next dark-green lithium atom. Blue polyhedrons show the lithium coordination around the single silicon atoms with bond length between 2.5 and 3.1 Å.

B. Structure obtained by EVO

This structure was generated with the evolutionary algorithm EVO [25], which was also able to find the crystal structure from the ICSD database. There are only small differences between them, which are displayed in Fig. 2. Between the light-green lithium atoms exits only minor changes, but if one moves the dark-green lithium atoms in the direction of the neighboring dark-green lithium atom and stops halfway, then one obtains the structure found by EVO. Now the silicon dimer has only four lithium atoms surrounding the Si-Si bond perpendicularly. The polyhedron of the silicon monomer has a

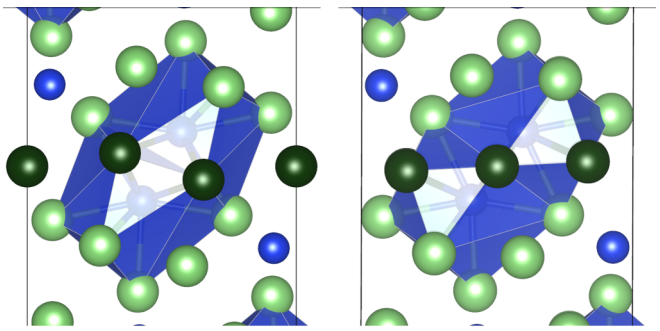

(a) from ICSD database (b) obtained with EVO

FIG. 2. Silicon dimer of $Li_{13}Si_4$ with c axis pointing toward the viewer (Li, light + dark green; Si, blue). Light reflections produces bright surfaces. Structures can be converted into each other by shifting the dark-green lithium atoms in the direction of the next dark-green lithium atom. Blue polyhedrons show the lithium coordination around the silicon dimer with bond length between 2.4 and 3.0 Å.

TABLE I. Wyckoff positions of specific lithium atoms

Atom from left to right	ICSD structure	EVO structure
First	2c	4g
Second	4g	2a
Third	4g	4g

slightly different deformation of the icosahedron compared to the one in the ICSD structure (Fig. 1). The dark-green marked lithium atoms have the Wyckoff positions shown in Table I.

The space group is the same and there are only slight differences in the cell parameters (Table II).

An interesting fact is that there was an earlier publication before Frank *et al.* on a Li_7Si_2 phase by Schäfer *et al.* [28]. Even if the Li:Si-ratio was different, most of the atom positions are the same. The main fact is that this structure has the same lithium constellation like the dark-green marked atoms of the EVO structure. Therefore, there is experimental evidence for the existence of this structure.

See Supplemental Material for the crystal structure file [27].

III. COMPUTATIONAL DETAILS

A. DFT calculations

The electronic structure calculations based on density functional theory were performed using the projected augmented wave (PAW) method [29] implemented in QUANTUMESPRESSO (QE) [30]. The PAW potentials were created by means of the atompaw code [31] with an exchange-correlation functional according to Perdew and Wang [32]. For lithium, the $1s$, $2s$, and $2p$ states are projectors and thus no core states were used. The PAW sphere radii were set to $2.2a_0$. For silicon the $3s$ and $3p$ projectors were used; $1s2s2p$ are core states and the PAW sphere radii were set to $1.5a_0$.

The kinetic energy cutoff was set to 952 eV for the plane wave basis set to obtain a convergence better than 2 meV atom^{-1}. In addition, a Monkhorst-Pack grid of $8 \times 4 \times 16$ for Brillouin zone integration was used, giving the same $\vec{k}$-point grid density in each direction. The self-consistency of total energy was set to 10^{-8} Ry.

The phonon wave numbers are obtained from a fully relaxed unit cell. The variable cell optimization was carried out with a convergence threshold on forces of 10^{-8} Ry a_0^{-1} and pressure on the unit cell below 0.1 kbar. The vibrational wave numbers have been calculated using perturbation theory [33] with a factor of two smaller $\vec{q}$ grid compared with the $\vec{k}$ grid. For comparison the same fully relaxed cell with the same convergence thresholds has been used for the finite displacement method. The PHONOPY code [34] was used to create $2 \times 2 \times 2$ supercells with finite displacements and the forces were then calculated with QE with a $4 \times 2 \times 8$ $\vec{k}$ grid. A $3 \times 3 \times 3$ supercell has been tested with a difference in the free energy up to 3.6 meV at 1000 K and a difference in the heat capacity up to 0.16 JK^{-1}mol^{-1}atom^{-1} at 70 K. Since the calculation time for the $3 \times 3 \times 3$ supercell is 30 times higher than for the $2 \times 2 \times 2$ supercell and the difference are small enough the $2 \times 2 \times 2$ supercell has been used.

TABLE II. Cell parameters of measured [26,46] and calculated unit cells. The z axis of the double cell is divided by two for comparison reason.

Structure	a (Å)	b (Å)	c (Å)	b/a	c/a	Volume (Å^3)
Frank *et al.* [26]	7.99(2)	15.21(3)	4.43(1)	1.904	0.554	538.37
Zeilinger *et al.* [5]	7.9488(4)	15.1248(8)	4.4661(2)	1.903	0.562	536.93(5)
ICSD	7.745	14.744	4.323	1.904	0.558	493.69
EVO	7.749	14.566	4.345	1.880	0.561	490.38
Double cell (z/2)	7.744	14.727	4.323	1.902	0.558	493.02

In order to calculate energy barriers, the nudged elastic band (NEB) method was used with the same convergence thresholds as in the variable cell optimization.

To observe the structural change, molecular dynamic simulations were carried out with QUANTUMESPRESSO. The convergence thresholds were lowered to allow for longer simulation times (kinetic energy cutoff 340 eV and $2 \times 1 \times 4$ $\vec{k}$ grid). To obtain the desired temperature the initial temperature was first doubled and then quenched to the desired temperature after several time steps. The simulation time for the calculations with temperatures of 700 K and below was about 220 ps and all other calculations 30 ps.

B. Calculation of thermodynamic properties

The free energy (F) is a central quantity in thermodynamics, which can be used to calculate other thermodynamic properties. It is defined as the sum of the inner energy (U_{tot}) and all entropic contributions. In particular, we focused on the vibrational (F_{vib}) and electronic (F_{el}) contributions, which are the dominating entropy-related contributions. Using perturbation theory or the finite-displacement method a phonon density of state ($D(\omega)$) has been obtained for the frequency range (ω). This phonon density of state contains the vibrational information for a specific volume (V) and can be used to calculate F_{vib} at any temperature (T) with the Planck (h) and Boltzmann constant ($\mathrm{k_b}$) [35]. The electronic density of states ($n(\epsilon,V)$) is used to calculate the electronic part F_{el}, which is the sum of the electronic energy (E_{el}) and the electronic entropy (S_{el}) [36]. It needs the Fermi-Dirac distribution (f) depending on the energy ϵ and the Fermi level $\mathrm{E_F}$:

$$F = U_{\mathrm{tot}}(V) + F_{\mathrm{vib}}(\omega(V),T) + F_{\mathrm{el}}(V,T), \tag{1}$$

$$F_{\mathrm{vib}} = \mathrm{k_B}T \int_{\omega} d\omega D(\omega) \ln\left(2\sinh\left[\frac{h\omega}{4\pi \mathrm{k_B}T}\right]\right), \tag{2}$$

$$F_{\mathrm{el}} = E_{\mathrm{el}} - T S_{\mathrm{el}}, \tag{3}$$

$$f = \left[\exp\left(\frac{\epsilon - E_{\mathrm{F}}}{\mathrm{k_B}T}\right) + 1\right]^{-1}, \tag{4}$$

$$E_{\mathrm{el}} = \int n(\epsilon,V) f \epsilon d\epsilon - \int^{E_{\mathrm{F}}} n(\epsilon,V)\epsilon d\epsilon, \tag{5}$$

$$S_{\mathrm{el}} = -\mathrm{k_B} \int n(\epsilon,V)[f \ln f + (1-f)\ln(1-f)]d\epsilon. \tag{6}$$

The free energy is calculated for at least five different volumes. Then the universal equation of state [37] has been used to find the minimum of the free energy over volume for a given fixed temperature. The procedure is then repeated for the whole temperature range. This gives a dependence of the volume corresponding to the minimum of the free energy on temperature. Thermodynamical properties like the specific heat capacity at constant pressure can then be calculated from this free-energy function as a second derivative.

The diffusion coefficient D can be calculated directly from the atomic movements during the MD simulation,

$$D = \frac{1}{6} \lim_{t\to\infty} \frac{\langle |\mathbf{r}_i(t) - \mathbf{r}_i(0)|^2 \rangle}{t}, \tag{7}$$

where $\langle\rangle$ denotes the average over the considered atoms, and $\mathbf{r}_i(t)$ is the position vector of the diffusing atom i at the time t. This equation works very well for gases and liquids. In case of solids with a specific jumping distance λ and a jump rate R the diffusion coefficient can be determined by [38]

$$D = \frac{\lambda^2 R}{2n}, \tag{8}$$

where n is the dimension of the diffusion. If a Li atom moves during the MD simulation from one lattice site to another one than the distance will change by more than 1 Å. We call such an event a "jump" and used this abrupt change of distance to identify jumps. This allows us to count the total number of jumps and by dividing with the simulation time it represents R used in Eq. (8). The mean distance for all jumps can be determined from the crystal structure and is denoted by λ. Assuming an Arrhenius behavior for the jump rate [39],

$$R = R_0 \cdot \exp\left(-\frac{E_{\mathrm{D}}}{\mathrm{k_b}T}\right), \tag{9}$$

we can obtain an activation barrier E_{D} from the temperature dependence of the jump rate R with the Boltzmann constant $\mathrm{k_b}$. A constant-energy MD simulation with initial temperature setting, no rescaling, second-order extrapolation, and a time step of 2.42 fs has been performed.

C. Evolutionary algorithm "EVO"

We developed an evolutionary algorithm to find new crystal structures that has been released as open source [25]. Parent structures were generated with random cell parameters and atom coordinates fulfilling certain chemical constrains. The number of atoms for each element is given in an input file. The parent structures undergo an evaluation by variable-cell structure relaxation with an external program like QE.

The fitness is determined from the enthalpy at 0 K. The first generation will be created by recombination of the parents. After evaluation of each individual too similar structures were

removed from the pool and the parents for the next generation will be selected from the best individuals.

The parameters for selection are set to generate a wide variety of offspring. For example, individuals will be removed if they survive a certain number of generation cycles so that they do not dominate the pool. From the new parent individuals the algorithm will continue with the next generation. At the end of the algorithm one gets the best structures from all generations. The code has already been used successful to find a new pure carbon structure with mixed sp^2 and sp^3 bonding [40] and tested on binary and ternary Mg-Si-O systems [41]. A detailed description of the method and parameters can be found in Ref. [25].

The "EVO" code generates the random structures and reads in the enthalpy of these structures to evaluate the next generation. The external program QE is used to optimize with a variable cell algorithm the random structures and calculates the enthalpy of them. The same cell size as the original one with 34 atoms is used to create from 15 parents 50 offspring over a maximum of 50 generations and is repeated three times. All cell angles are between 45° and 135°, and no other cell constrain is set for the random structure generation.

IV. RESULTS AND DISCUSSION

A. Stability of the two structures

The dynamical stability of both structures can be verified by phonon calculations, because all phonon frequencies should be positive for stability. Interestingly, this is not true for both structures (Fig. 3). This was also observed by Chevrier [42] and attributed it to the lithium motion. For verification, the phonon DOS of the relaxed volume has been calculated with both methods explained in Sec. III, finite displacement method and linear response techniques based on perturbation theory. The phonon dispersion, the phonon DOS (Fig. 13) and the free energy of both methods are very similar. Since the finite displacement method is ten times faster for these systems, we decided to choose this method to calculate the free energy and other thermodynamic properties.

Every three-dimensional crystal has exactly three acoustic modes, which are zero after applying the acoustic sum rule. In the single-unit cell the ICSD structure has at the Γ point three modes with zero frequency, but the EVO structure has an additional fourth mode close to zero. The displacement pattern of this fourth mode is almost identical between both methods. Using the linear response method the frequency obtained is 23i cm^{-1} compared to 15 cm^{-1} with the finite displacement method. For verification the energy as a function of the frozen phonon displacement has been calculated. For a real instability one would expect a saddle point or a concave function, which is not found here but rather a strong anharmonic potential, which fits well to a polynomial of fourth order (Fig. 4).

The polynominal fit of the energy curve is then used as the potential for the numerical solution of an anharmonic quantum mechanical oscillator. The lowest excitation for this mode is 22 cm^{-1} and fits better to the frequency of the finite displacement pattern compared to the one of the linear response method. Both methods are not accurate enough to estimate the origin of these quartic contributions. The self-consistent phonon theory [43–45] would be a better choice, but beyond the scope of the current work.

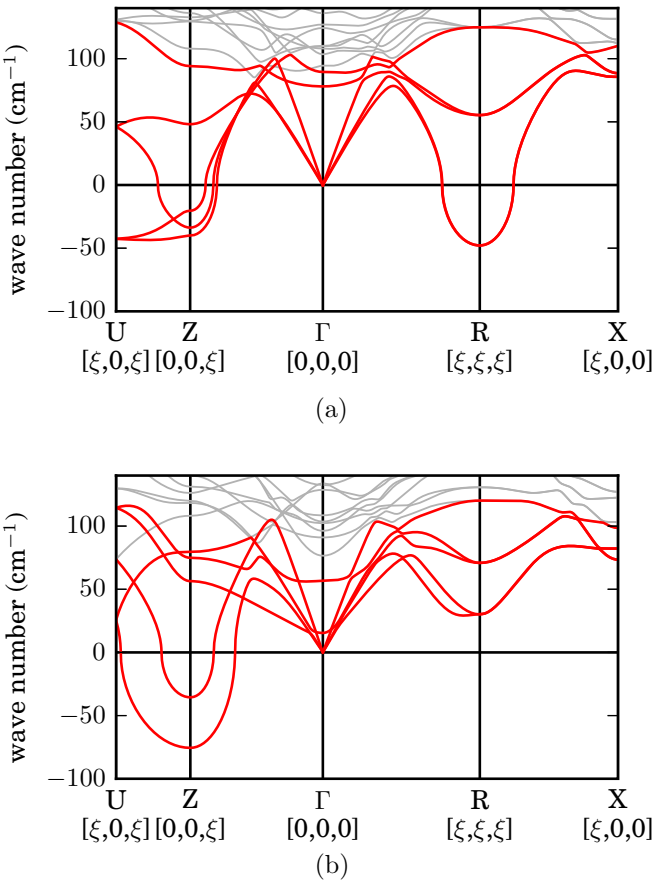

FIG. 3. Comparison of the phonon dispersion of the (a) ICSD structure and the (b) EVO structure calculated with the finite displacement method. Lowest five bands are highlighted in red for clarity.

Conclusions about instability can be best made from the phonon dispersion. In general the phonon dispersions (Fig. 3) and phonon DOS (Fig. 14) for both structures are similar, but indicate some differences of the highest modes and the imaginary ones. Both structures have no imaginary phonon modes at the Γ-point, but imaginary phonon modes at the Z point ([0,0,0.5]). The ICSD structure has also some imaginary phonon modes at the R point ([0.5,0.5,0.5]), which contains also a Z component. Surprisingly, these imaginary modes disappear when the volume increases (Fig. 5). At a certain volume corresponding to a certain temperature all phonon modes will be positive. This is true for the ICSD structure at a smaller volume expansion compared with the EVO structure. It seems that the increase in atom distance can stabilize the phonon mode.

Imaginary phonon modes along the [0,0,0.5] direction can be due to unoptimized atom positions within a double-unit cell along the c direction. To verify this, the unit cell was doubled in the c direction and the phonon mode with the highest imaginary frequency was used to displace all atoms described by this mode. Then a structure optimization of the new unit cell with twice as much atoms was carried out. The phonon dispersion of this optimized bigger unit cell shows no

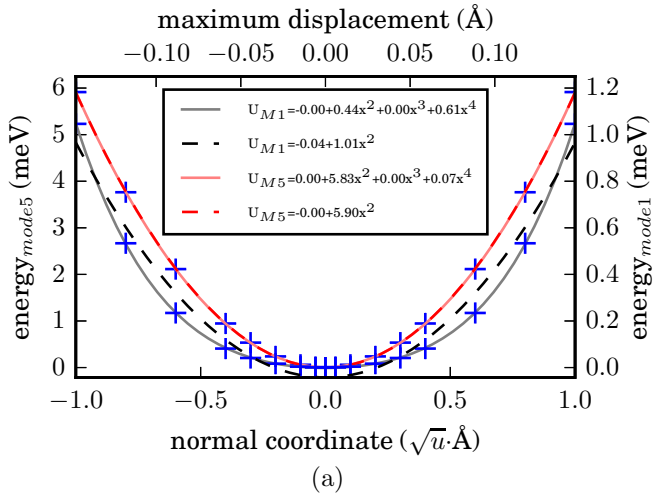

(a)

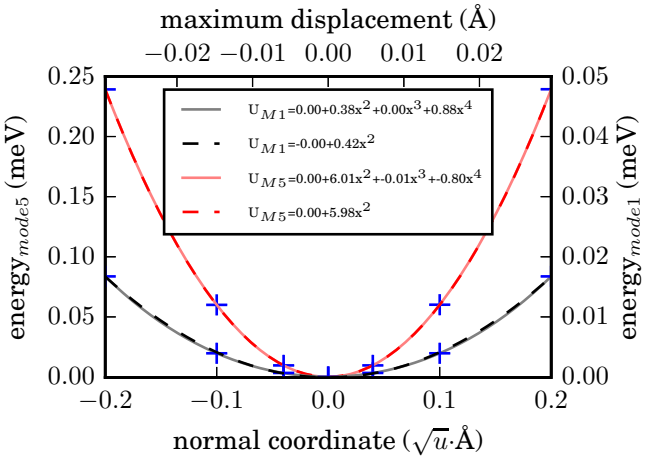

(b)

FIG. 4. Potential curves of the frozen phonon displacement of the 1 and 5 (for comparison) mode for (a) big and (b) small displacements with harmonic (solid line) and anharmonic (dashed line) polynomial fit. The displacement pattern from the EVO structure calculated with the linear response method was used.

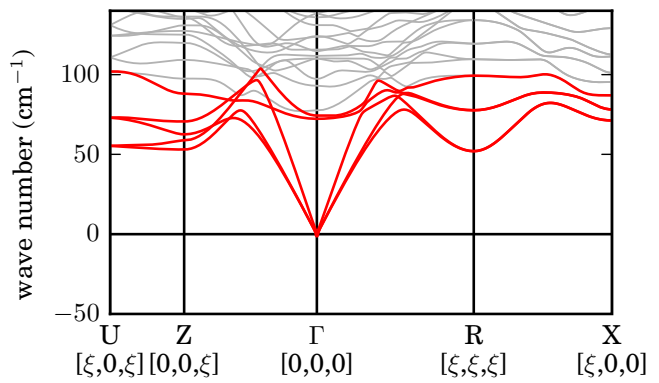

FIG. 5. Phonon dispersion of the ICSD structure with 5% isotropic increase of all cell axis. Lowest five bands are highlighted in red for clarity.

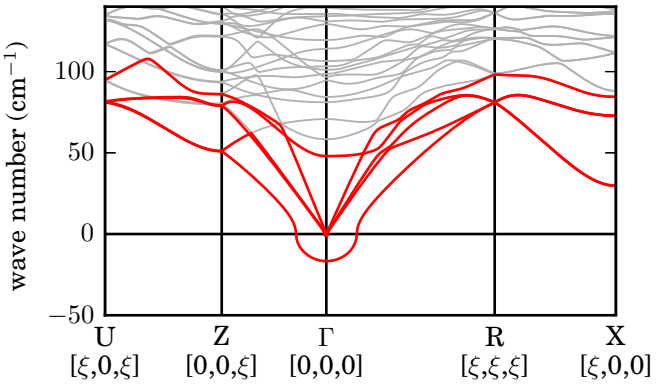

FIG. 6. Phonon dispersion of the ICSD structure with the double-unit cell in the c direction. Lowest five bands are highlighted in red for clarity.

imaginary frequencies, except for the Γ point (Fig. 6). See Supplemental Material for the crystal structure file [27].

By comparing the phonon dispersion of the single cell [Fig. 3(a)] with the double cell (Fig. 6), one may notice that the three lowest phonon modes in the single cell show a maximum at halfway from Γ to Z and to R. This could be a sign of a symmetry and if we half the Brillouin zone by using a double cell the phonon modes now increase monotonously. From the phonon calculation we can now say that this corresponds to a vibrationally stable unit cell. The structural difference compared to the ICSD structure is that some atoms lay no longer perfectly in the ab plane and display an offset in the c direction. This displacement can be supported by the single crystal x-ray diffraction measurement of Zeilinger *et al.* [46]. They show for these atoms displaced in c direction an anisotropy of the charge density along this direction. Even for the ones displaced in the ab plane exist equivalent anisotropies. The measured charge-density anisotropy can be explained very well by this doubled unit cell. Therefore, using a larger cell solves the discrepancy between theory and experiment.

After exploring the origin of the unstable phonon modes in the calculations, one can now compare the measured and calculated unit cells. Since LDA pseudopotentials are used, the calculated volume is smaller than the experimental one (Table II). By comparing the cell parameters one can see that the b axis of the EVO unit cell is smaller than the other, which can be seen in the b/a ratio, too. The c/a ratio of the calculated cells is between the two measured unit cells. In general, the calculated ratios are in the same range as the measured ones and the ISCD structure fits a little better. By scaling the cell axis to obtain the same volume as in the experiment, one can compare the simulated XRD structures directly to experimental data obtained by Thomas *et al.* [47] (Fig. 7). The simulated spectrum from the doubled cell has not been included, since it is almost identical to the ICSD spectrum.

Some reflexes fit better to the EVO structure (around 40°). However, reflexes around 43.1° or 25.9° are worse. The reflex at 16.0° is not present and the reflexes around 38° are more intense compared to the ICSD spectrum. In general, the simulated spectrum from the ICSD structure fits better to experiment than the EVO structure. If one simulates both

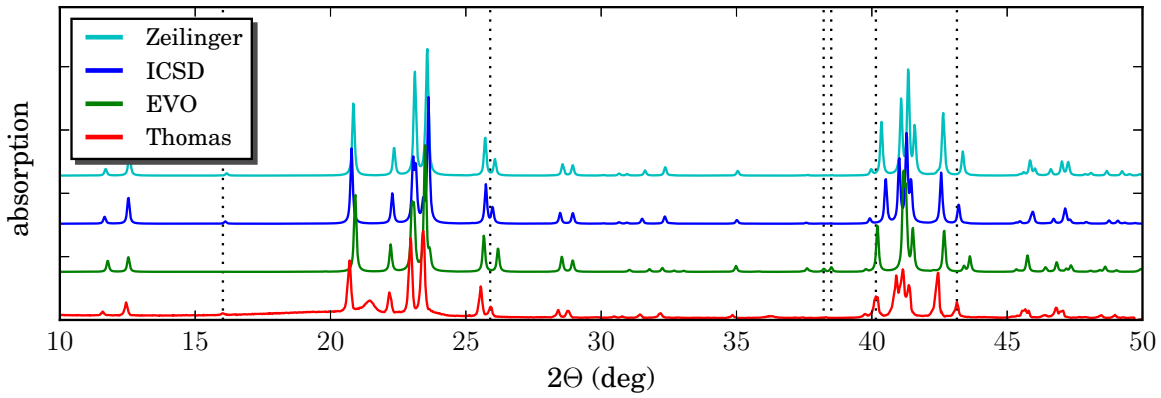

FIG. 7. Comparison of experimental data from Thomas [47] and simulated XRD spectra of the unit cell from Zeilinger *et al.* [46] and from scaled calculated unit cells (ICSD + EVO) to the volume of the structure from Zeilinger.

structures with the same unit cell setting, then the reflexes are almost identical. There are only slight changes in the intensities. The cell parameters between these two structures differ by up to 1.2% and the reflexes can change up to 0.4°. A refinement of the cell parameter can result in a better fit, but it looks as if the perfect cell has not been found yet. Please note that the measured sample is eventually a mixture of the two described phases. The reflexes of the simulated spectrum from the Zeilinger *et al.* unit cell are between the reflexes of the two calculated unit cells, but it differs from the Thomas [47] measured XRD spectrum, too. It seems that the XRD spectrum from Thomas *et al.* [47] cannot be simulated perfectly by one of these unit cells.

The phonon calculations show that both phases are stable and the XRD spectrum can not clarify which of the two phases may be present. Therefore, a mixture of both phases is possible and a phase transition may be considered. The free energy can be calculated from the phonon density of state [Eq. (1)] and can determine which phase is more stable within the temperature range, since at atmospheric pressure it is almost identical to the Gibbs energy. At zero Kelvin the free energy for the ICSD structure is lower than the one from the EVO structure by 68 meV per unit cell as already determined from the cell optimization. The zero-point motion energy for both phases is 53.8 meV with a difference of smaller than 0.1 meV. However, F_{vib} decreases faster for the EVO structure than U_{tot} increases for the ICSD structure. It overcompensates this and at high temperature the EVO structure has a lower free energy than the ICSD structure. But the free energy is not the only parameter that determines which phase would be present at a certain temperature. It could also be possible that both phases exist next to each other, but in a changing ratio over the temperature range. A closer look at the fourth phonon band close to zero at the Γ point of the EVO structure reveals something interesting. The vibrational mode acts on the six lithium atoms marked dark green in Fig. 2(b). If one moves the atoms along the acting forces, a subsequent relaxation will create the ICSD structure. This means that this vibrational mode indicates a phase transition pathway between these two structures.

Phase transitions and lithium movements produce entropy and will effect the heat capacity. The measured heat capacity by Thomas *et al.* [47] is compared with the calculated heat capacity for both structures, including the vibrational and electronic contributions [Eq. (1), Fig. 8]. The comparison of the calculated heat capacity with experimental data for the elements lithium and silicon shows a very good agreement up to near the melting point. This proves the accuracy of the calculated data and that no other significant effects play a role. For the $Li_{13}Si_4$ phase in Fig. 8 there is a good agreement between all curves at low temperatures, but a clear deviation between theory and experiment [47] at higher temperatures.

Missing entropic effects in the calculation could be due to vacancies or disorder. Vacancies, for example, would increase c_p exponentially just before the melting point [48,49] and not linearly over a wide temperature range. However, lithium vacancy formation has according to our DFT calculations a rather high energy cost of the order of one eV. At the same time, the DFT calculations indicate that the free-energy difference between the two structures discussed is only 68 meV per unit cell and decreases with increasing temperature. The existence of two phases very close in energy can cause disorder, which also would increase the heat capacity.

To conclude the stability analysis, there is evidence of the existence for two possibly stable structures. The true unit cell is twice as big and has no longer imaginary modes except for the Γ point, but the calculation takes about 15 times longer. Since the effect of the imaginary modes to the heat capacity is not significant, the free energy is calculated with

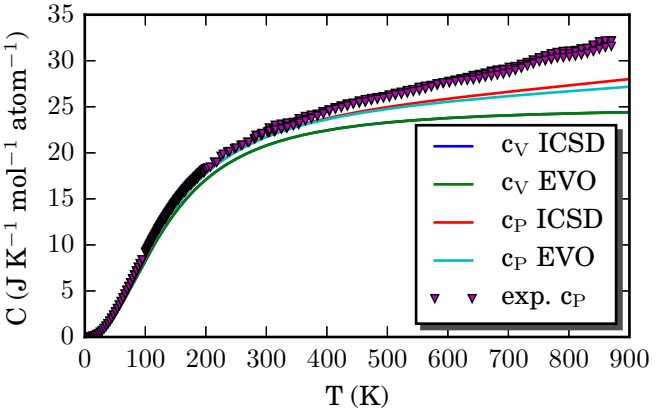

FIG. 8. c_V and c_P of $Li_{13}Si_4$ structures.

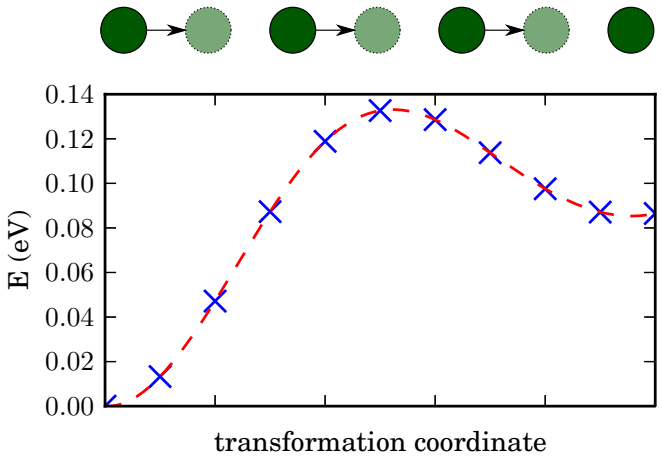

FIG. 9. Energy barrier for phase transition from ICSD to EVO structure at 0 K. The above circles mark the moving dark-green lithium atoms (Fig. 2), from the ICSD to the EVO positions.

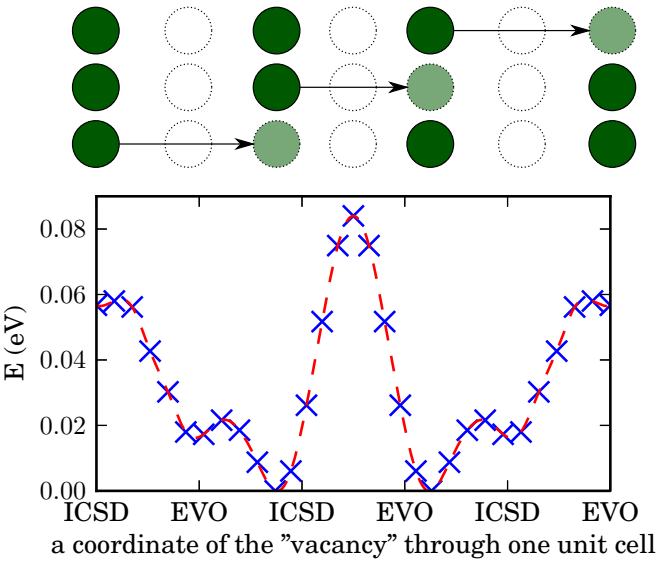

FIG. 10. Energy curve of a vacancy movement through the unit cell along the a axis at 0 K. The x coordinate marked with ICSD (EVO) are the lithium positions in the ICSD (EVO) structure. The above circles mark the moving dark green lithium atoms (Fig. 2), starting from the ICSD positions.

the single-unit cells for both structures. There exists a fourth phonon band close to zero at the Γ point of the EVO structure, which describes the atom movement along the phase transition pathway between the two structures. This mode decreases and becomes slightly imaginary with increasing volume. The free energy reveals a very small and decreasing energy difference with increasing temperature between the two phases and the heat capacity measurement indicates some still unknown entropic effect above room temperature. There are many signs for a phase transition and the following section will give a detailed analysis of such a possibility.

B. Phase transition

As discussed in the previous section there is a continuous transformation between the two structures by moving the dark green atoms shown in Fig. 2. First, the phase transition was investigated with the nudged elastic band method using the whole unit cell in order to estimate the energy barriers involved. This energy curve has been calculated at 0 K and constant volume of the ICSD structure. This means that the energy for the EVO structure is a little bit higher than 68 meV per unit cell given for the fully relaxed cell since the relaxed volume is smaller.

As can be seen in Fig. 9 there is a clear barrier between the two structures. The data displayed here has been obtained by moving all atoms from the fractional coordinates in the ICSD structure to the fractional coordinates in the EVO structure with the NEB method. The resulting barrier is 133 meV with an energy difference between the ICSD and EVO structure of about 86 meV. The obtained energy barrier of 133 meV is very low and can be compared to the one found in $Li_{12}Si_7$. In this phase an ultrafast quasi-1D diffusion was measured by Kuhn *et al.*[24] with a diffusion barrier of 180 meV.

However, the phase transition can proceed in several steps due to the movement of more than one lithium atom at the same time. This effect can be seen in Fig. 10. To get a deeper insight into the lithium movement a second NEB calculation has been carried out with the introduction of a lithium vacancy instead of one of the three dark-green marked atoms in Fig. 2. One neighboring lithium atom was then moved from its original position to the vacancy. The potential energy curve is constructed by collecting the data from three calculations with the vacancy at the three different positions. This curve is similar to the lithium movement of one lithium atom through the whole unit cell passing all lithium positions of both structures (Fig. 10). One can see that there are two deep and two shallow minima, which correspond to the ICSD or EVO structures. Please note that the barriers are rather small with only several tens of meV, which means that there is practically no thermal activation needed for a transformation between the structures. The third lithium atom of each structure has an unstable position and a transition to the neighboring position could stabilize this atom. Unfortunately, one new unstable lithium position would be created.

The experimental situation is not clear yet. Dupke *et al.* [50] observed in a differential scanning calorimetry experiment a phase transition at 145 K. However, in the work of Thomas [47], no peak as a sign for a phase transition has been observed.

C. Results of the molecular dynamic simulations

Molecular dynamic (MD) simulations can help to determine phase transitions [51]. Starting from the ICSD structure, MD simulations were done at several temperatures (300 K, 400 K, 450 K, 500 K, 550 K, 600 K, 650 K, 700 K, 750 K, 800 K, 900 K, 1050 K, and 1500 K). In each case lithium mobility corresponding to jumps between positions identified with the NEB method has been found. Below 750 K only the six specified lithium atoms (marked as dark green in Fig. 1) in the unit cell show a significant diffusion coefficient. Above 700 K more lithium atoms start to move, but the silicon atoms still show no diffusion within the first 30 ps. At 1500 K the structure becomes unstable and all atoms leave their relaxed position.

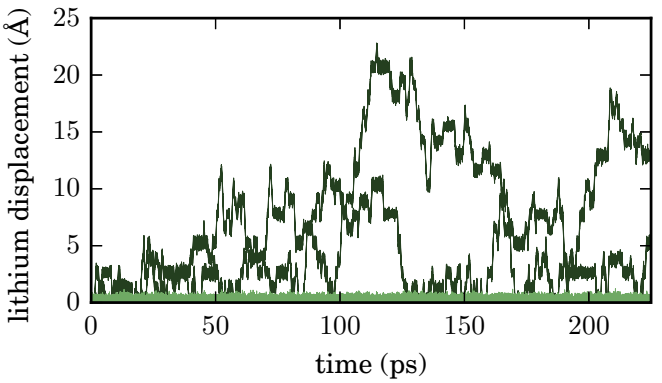

FIG. 11. Absolute displacement for each lithium atom in the unit cell at 450 K. Distance between each jump is 1.29 Å. Each line represents one lithium atom and is colored as described in the caption of Fig. 1.

A closer look at the MD simulations up to 700 K reveals that the lithium atoms move concerted in groups of three. The dark-green marked atoms in Fig. 2 that are direct neighbors are in groups of three and exactly these groups are moving at once. The lithium atoms can stay for a certain time at a position and then switch from the ICSD wyckoff positions to the next EVO wyckoff positions or the other way around. It is also possible that the lithium atoms jump directly to the next ICSD positions and even further (Fig. 11). All light-green lithium atoms linger at their equilibrium positions. The dark-green atoms oscillate around a certain displacement to its equilibrium position before it jumps to a new displacement. The difference between each possible oscillating displacement is always 1.29 Å, which is the distance between the dark-green atoms of the EVO and ICSD structure.

When the atoms move from the ICSD to the EVO positions or vice versa, then we count this as a single jump. Double jumps would be from one ICSD to the next ICSD positions. From the MD calculation with one unit cell the jumps per picoseconds are listed in Table III, and the ratio between single and double jumps slightly decreases with increasing temperature. Therefore, with increasing temperature the jump rate and jumping distance increases, and the duration of the atoms to linger at their positions decreases. But the duration time in a position decreases faster for the ICSD structure than for the EVO structure and is almost equal at 700 K. Above 700 K the EVO structure appears to be preferred. This goes along with the free energy calculated earlier, where the free energy of the EVO structure becomes more favorable with increasing temperature.

These MD simulations suggest that the two structures can appear at the same time and that temperature controls which structure is preferred. This dynamic process can be compared with the chemical description of a resonance stabilization through back and forth jumping of specific lithium atoms. It could also be considered as a quantum mechanical two-level system, in which energies are more or less degenerated. This two-level system creates a new state lowered in energy compared to the two separated states and the phase transition can be regarded as the interaction between the two states. The driving force would be the existence of unstable lithium position in both structures.

During the phase transition the three moving lithium atoms move concerted with the three lithium atoms in the neighboring unit cell and this lithium movement can be seen as a one-dimensional diffusion along the a axis. The MD simulation allows us to determine diffusion coefficients [Eq. (7)]. In our case D does not increase monotonously with temperature (Table III). The diffusion coefficients depend strongly on the direction the lithium atoms jump. Unfortunately, even 220 ps seems not to be long enough for a reliable estimate. However, by plotting the logarithm of the jump rate over $1/T$ [Eq. (9)], one obtains a perfect line (Fig. 12).

The jump rate R is determined by counting all jumps in each simulation as single jumps divided by the simulation time. A double jump would be counted as two single jumps. From the slope one can obtain an activation energy [39] E_{D} of 64 meV. Since this activation energy represents the jump for one out of two lithium constellations in the unit cell, the activation energy for the whole unit cell is 128 meV, which is very close to the barrier we obtained from the NEB calculation. The diffusion coefficient is directly related to the jump rate R by $D = \lambda^2 R/(2n)$ [38] [Eq. (8)], where λ is the average distance of 1.29 Å with $n = 1$ for a one-dimensional diffusion (Table III). The diffusion coefficients represent the ideal case, if every jump would be in the same direction. Using the just

TABLE III. Results from the MD calculations with a single ICSD unit cell as the starting structure. Temperature is the average temperature of the run. Jumps from ICSD wyckoff positions to the next EVO positions are counted as single jumps (Single j.). The duration (Dur.) is the time that the atoms stay in a certain position. The time (t) represents the percentage the atoms are at the ICSD positions. The diffusion coefficient D has been obtained from the MD directly or calculated from the jump rate (jumpr).

T (K)	Single j. (ps^{-1})	Double j. (ps^{-1})	Dur. (ICSD) (ps)	Dur. (EVO) (ps)	t (ICSD)	D (MD) (10^{-6} cm^2 s^{-1})	D (jumpr) (10^{-6} cm^2 s^{-1})
319.9	0.440	0.109	4.322	2.138	70.8%	2.46	33.45
415.2	0.708	0.182	2.274	1.670	63.0%	14.57	58.33
461.2	0.987	0.212	1.715	1.334	58.4%	4.78	72.07
512.4	0.924	0.271	1.728	1.207	60.1%	29.73	81.21
563.4	1.074	0.329	1.441	1.128	61.8%	11.86	90.66
615.6	1.207	0.319	1.302	1.075	55.3%	17.18	98.83
667.0	1.366	0.421	1.047	0.991	53.1%	15.36	116.35
719.4	1.254	0.508	1.021	0.998	47.6%	20.34	123.24

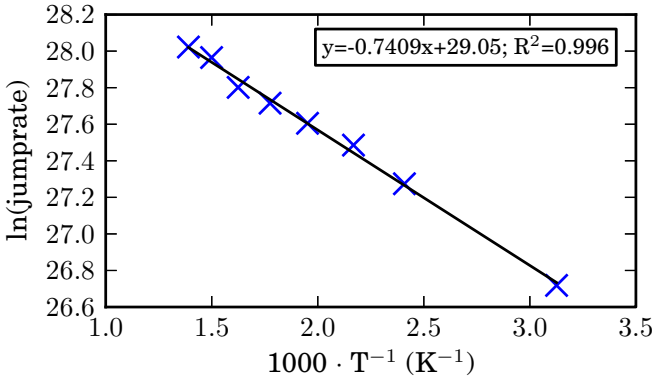

FIG. 12. Determination of the activation energy by using the jump rate (s^{-1}) per unit cell.

obtained values for D and E_D we obtain a prefactor D_0 of 3.10^{-4} cm^2 s^{-1}.

V. CONCLUSION

According to our MD simulations, the $Li_{13}Si_4$ phase may exist in two different forms. One previously known from the ICSD database and a new one found by our evolutionary algorithm EVO. The previously reported imaginary phonon frequencies as a sign for instability is due to a too small unit cell size. The true unit cell is doubled in the c direction.

The analysis of the phonon modes and molecular dynamic simulations reveal a transition between these two structures. In both structures some lithium atoms have unstable positions and this is a driving force for the phase transition. This could be considered as an interaction between a two-level system to create a more stabilized system. This transition does not occur at a definite temperature but resembles more an equilibrium between the structures, which will shift with increasing temperature from the ICSD to the EVO structure. The ICSD structure is at low temperature more stable than the EVO structure. These two structures are intermediate structures of a very rapid one-dimensional lithium diffusion along the a axis. This can clearly be observed during an MD simulation in the temperature range up to 700 K, before other lithium atoms start to move. The energy barrier determined from the jump rate is 64 meV and can easily be overcome by thermal excitation below room temperature. This energy barrier is very close to the transition barrier of 66 meV determined by the nudged elastic band method, since there are two independent lithium pathways in the unit cell.

ACKNOWLEDGMENTS

This work was financially supported by the DFG-SPP 1473 *WeNDeLIB*. The authors thank the ZIH TU-Dresden, the Cluster of Excellence "Structure Design of Novel High-Performance Materials via Atomic Design and Defect Engineering (ADDE)" that is financially supported by the European Union (European regional development fund) and by the Ministry of Science, and the URZ of TU Bergakademie Freiberg for providing computer resources, technical expertise, and assistance.

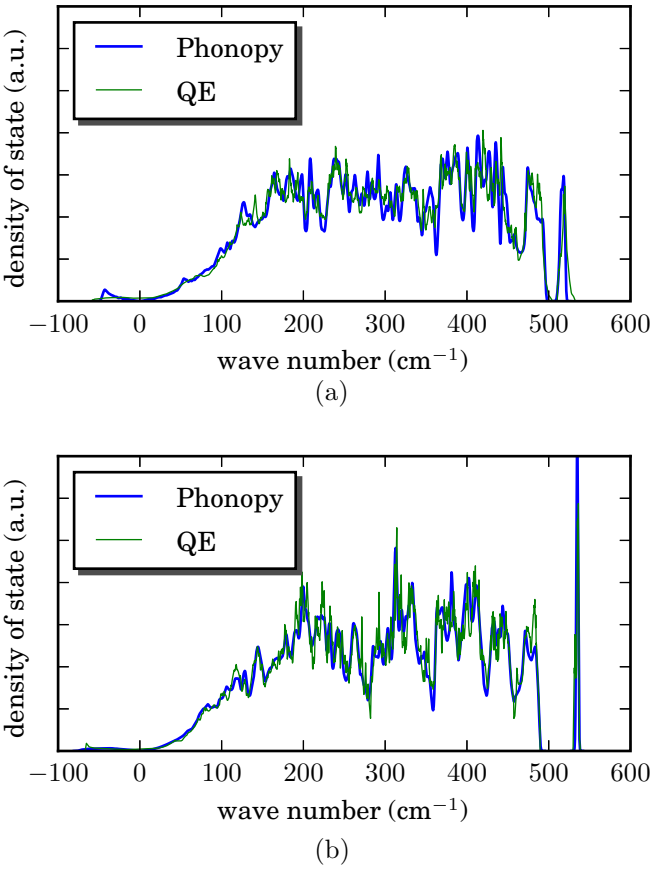

FIG. 13. Comparison of the phonon density of state (DOS) of the (a) ICSD and (b) EVO structure calculated with perturbation theory and finite displacement method.

APPENDIX

Two methods were tested for the phonon calculations. The comparison of the perturbation theory with the finite displacement method was performed on the basis of the phonon density of state (DOS) for both structures of the $Li_{13}Si_4$ phase (Fig. 13). The two methods result in almost identical phonon DOS. By comparing the phonon DOS of the two structures among each other small differences can be observed (Fig. 14).

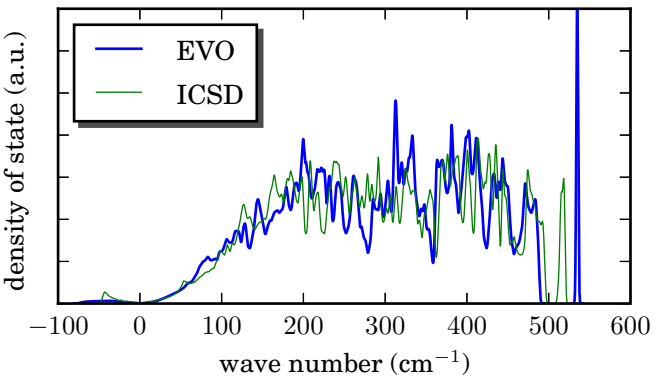

FIG. 14. Comparison of the phonon density of states (DOS) of the two structures obtained by perturbation theory.

[1] J.-M. Tarascon and M. Armand, Nature **414**, 359 (2001).
[2] B. Kang and G. Ceder, Nature **458**, 190 (2009).
[3] M. Park, X. Zhang, M. Chung, G. B. Less, and A. M. Sastry, J. Power Sources **195**, 7904 (2010).
[4] C.-M. Wang, X. Li, Z. Wang, W. Xu, J. Liu, F. Gao, L. Kovarik, J.-G. Zhang, J. Howe, D. J. Burton *et al.*, Nano Lett. **12**, 1624 (2012).
[5] M. Zeilinger, D. Benson, U. Häussermann, and T. F. Fässler, Chem. Mater. **25**, 1960 (2013).
[6] J. L. Goldman, B. R. Long, A. A. Gewirth, and R. G. Nuzzo, Adv. Funct. Mater. **21**, 2412 (2011).
[7] Y.-M. Kang, S.-B. Suh, and Y.-S. Kim, Inorg. Chem. **48**, 11631 (2009).
[8] M. N. Obrovac and L. Christensen, Electrochem. Solid-State Lett. **7**, A93 (2004).
[9] M. N. Obrovac and L. J. Krause, J. Electrochem. Soc. **154**, A103 (2007).
[10] S. K. Soni, B. W. Sheldon, X. Xiao, A. F. Bower, and M. W. Verbrugge, J. Electrochem. Soc. **159**, A1520 (2012).
[11] A. S. Cattaneo, S. Dupke, A. Schmitz, J. P. Badillo, M. Winter, H. Wiggers, and H. Eckert, Solid State Ionics **249-250**, 41 (2013).
[12] J.-H. Trill, C. Tao, M. Winter, S. Passerini, and H. Eckert, J. Solid State Electrochem. **15**, 349 (2011).
[13] P. Wang, A. Kozlov, D. Thomas, F. Mertens, and R. Schmid-Fetzer, Intermetallics **42**, 137 (2013).
[14] W. W. Tipton, C. R. Bealing, K. Mathew, and R. G. Hennig, Phys. Rev. B **87**, 184114 (2013).
[15] V. L. Chevrier and J. R. Dahn, J. Electrochem. Soc. **156**, A454 (2009).
[16] V. L. Chevrier and J. R. Dahn, J. Electrochem. Soc. **157**, A392 (2010).
[17] C.-Y. Chou and G. S. Hwang, Surface Science **612**, 16 (2013).
[18] W. Wan, Q. Zhang, Y. Cui, and E. Wang, J. Phys.: Condens. Matter **22**, 415501 (2010).
[19] Q. Zhang, W. Zhang, W. Wan, Y. Cui, and E. Wang, Nano Lett. **10**, 3243 (2010).
[20] M. K. Y. Chan, C. Wolverton, and J. P. Greeley, J. Am. Chem. Soc. **134**, 14362 (2012).
[21] Y. Okamoto, J. Phys. Chem. C **115**, 25160 (2011).
[22] P. Johari, Y. Qi, and V. B. Shenoy, Nano Lett. **11**, 5494 (2011).
[23] Q. Zhang, Y. Cui, and E. Wang, Modell. Simul. Mater. Sci. Eng. **21**, 074001 (2013).
[24] A. Kuhn, P. Sreeraj, R. Pöttgen, H.-D. Wiemhöfer, M. Wilkening, and P. Heitjans, J. Am. Chem. Soc. **133**, 11018 (2011).
[25] S. Bahmann and J. Kortus, Comput. Phys. Commun. **184**, 1618 (2013).
[26] U. Frank, W. Müller, and H. Schaefer, Z. Naturforsch., B: Anorg. Chem., Org. Chem. **30**, 10 (1975).
[27] See Supplemental Material at http://link.aps.org/supplemental/10.1103/PhysRevB.93.144104 for crystal structure file.
[28] H. Schaefer, H. Axel, and A. Weiss, Z. Naturforsch., B: Anorg. Chem., Org. Chem. **20**, 1010 (1965).
[29] P. E. Blöchl, Phys. Rev. B **50**, 17953 (1994).
[30] P. Giannozzi, S. Baroni, N. Bonini, M. Calandra, R. Car, C. Cavazzoni, D. Ceresoli, G. L. Chiarotti, M. Cococcioni, I. Dabo *et al.*, J. Phys.: Condens. Matter **21**, 395502 (2009).
[31] N. A. W. Holzwarth, A. R. Tackett, and G. E. Matthews, Comput. Phys. Commun. **135**, 329 (2001).
[32] J. P. Perdew and Y. Wang, Phys. Rev. B **45**, 13244 (1992).
[33] P. Giannozzi, S. de Gironcoli, P. Pavone, and S. Baroni, Phys. Rev. B **43**, 7231 (1991).
[34] A. Togo, F. Oba, and I. Tanaka, Phys. Rev. B **78**, 134106 (2008).
[35] M. T. Dove, *Introduction to Lattice Dynamics*, Vol. 4 (Cambridge University Press, Cambridge, 1993).
[36] Y. Wang, Z.-K. Liu, and L.-Q. Chen, Acta Mater. **52**, 2665 (2004).
[37] P. Vinet, J. H. Rose, J. Ferrante, and J. R. Smith, J. Phys.: Condens. Matter **1**, 1941 (1989).
[38] E. Ganz, S. K. Theiss, I.-S. Hwang, and J. Golovchenko, Phys. Rev. Lett. **68**, 1567 (1992).
[39] X.-P. Tang, U. Geyer, R. Busch, W. L. Johnson, and Y. Wu, Nature **402**, 160 (1999).
[40] S. Bahmann, T. Weißbach, and J. Kortus, Phys. Status Solidi RRL **7**, 639 (2013).
[41] S. Bahmann, Ph.D. thesis, TU Bergakademie Freiberg, 2014, http://www.qucosa.de/recherche/frontdoor/?tx_slubopus4frontend[id]=urn:nbn:de:bsz:105-qucosa-141596.
[42] V. Chevrier, J. Zwanziger, and J. Dahn, J. Alloys Compd. **496**, 25 (2010).
[43] N. R. Werthamer, Phys. Rev. B **1**, 572 (1970).
[44] M. L. Klein and G. K. Horton, J. Low Temp. Phys. **9**, 151 (1972).
[45] I. Errea, M. Calandra, and F. Mauri, Phys. Rev. B **89**, 064302 (2014).
[46] M. Zeilinger and T. F. Fässler, Acta Crystallogr. Sect. E **69**, i81 (2013).
[47] D. Thomas, M. Abdel-Hafiez, T. Gruber, R. Hüttl, J. Seidel, A. U. Wolter, B. Büchner, J. Kortus, and F. Mertens, J. Chem. Thermodyn. **64**, 205 (2013).
[48] B. Grabowski, L. Ismer, T. Hickel, and J. Neugebauer, Phys. Rev. B **79**, 134106 (2009).
[49] R. W. Christy and A. W. Lawson, J. Chem. Phys. **19**, 517 (1951).
[50] S. Dupke, T. Langer, R. Pottgen, M. Winter, S. Passerini, and H. Eckert, Phys. Chem. Chem. Phys. **14**, 6496 (2012).
[51] S. Schmerler and J. Kortus, Phys. Rev. B **89**, 064109 (2014).